1-1-2015

Nano-carbon electrodes for thermal energy harvesting

Mark S. Romano
University of Wollongong, mromano@uow.edu.au

Joselito M. Razal
Deakin University, University of Wollongong, jrazal@uow.edu.au

Dennis Antiohos
University of Wollongong, dennisa@uow.edu.au

Gordon G. Wallace
University of Wollongong, gwallace@uow.edu.au

Jun Chen
University of Wollongong, junc@uow.edu.au

Nano-carbon electrodes for thermal energy harvesting

Abstract

Thermogalvanic cells are capable of converting waste heat (generated as a by-product of almost all human activity) to electricity. These devices may alleviate the problems associated with the use of fossil fuels to meet the world's current demand for energy. This review discusses the developments in thermogalvanic systems attained through the use of nano-carbons as the electrode materials. Advances in cell design and electrode configuration that improve performance of these thermo converters and make them applicable in a variety of environments are also summarized. It is the aim of this review to act as a channel for further developments in thermogalvanic cell design and electrode engineering.

Keywords

electrodes, nano, harvesting, energy, thermal, carbon

Disciplines

Engineering | Physical Sciences and Mathematics

Publication Details

Romano, M. S., Razal, J. M., Antiohos, D., Wallace, G. & Chen, J. (2015). Nano-carbon electrodes for thermal energy harvesting. Journal of Nanoscience and Nanotechnology, 15 (1), 1-14.

Nano-Carbon Electrodes for Thermal Energy Harvesting

Mark Romano, Joselito M. Razal, Dennis Antiohos, Gordon Wallace*, and Jun Chen*

Intelligent Polymer Research Institute, ARC Centre of Excellence for Electromaterials Science, Australian Institute of Innovative Materials, Innovation Campus, University of Wollongong, Northfields Avenue, Wollongong, NSW 2522, Australia

Thermogalvanic cells are capable of converting waste heat (generated as a by-product of almost all human activity) to electricity. These devices may alleviate the problems associated with the use of fossil fuels to meet the world's current demand for energy. This review discusses the developments in thermogalvanic systems attained through the use of nano-carbons as the electrode materials. Advances in cell design and electrode configuration that improve performance of these thermo converters and make them applicable in a variety of environments are also summarized. It is the aim of this review to act as a channel for further developments in thermogalvanic cell design and electrode engineering.

Keywords: Thermogalvanic Cells, Thermocells, Thermo-Electrochemical Cells, Low-Grade Heat, Waste Heat Carbon Nanotubes, Graphene, Reduced Graphene Oxide.

CONTENTS

1. INTRODUCTION

1.1. The World's Energy Problem

The availability of energy is crucial in economic development as has been shown in past studies.[1] Increased energy consumption is becoming necessary to generate (and sustain) more wealth, as can be seen in the correlation of greater production output through the use of high powered automated machines and equipment. This is depicted in Figure 1 which shows the growing rate at which energy is being consumed between 1982 to 2007.[2] Most of the world's energy comes from fossil fuels (coal, oils, and gas). Burning of these fuels has a negative environmental impact, from CO_2 emissions to global warming.[3] With the increasing rate of energy consumption, especially in developing countries, the finite nature of these resources presents an additional problem.[4] Technological improvements in renewable energy sources may lead to a decrease in the use of fossil fuels. Furthermore, alternative energy sources need to be developed in order to sustain the quality of life we have currently attained and to facilitate future economic development.[5] One such source is thermal energy, which may be obtained from geothermal sources and as a by-product of almost all human activity.

1.2. Various Unharnessed Waste Heat Sources

Low grade heat (normally around 130 $^{\times}$C) or waste heat is produced in our everyday activities, particularly during energy conversion. For example, when thermal energy is transduced to mechanical work by heat engines, excess heat is always produced. This fact is supported by the second law of thermodynamics, which states that no heat engine can attain 100% efficiency.[6] By simply turning on a car engine, waste heat is created and dissipated into the environment via a hot exhaust pipe. Another example

Mark Romano received his M.S. degree in Materials Science Engineering from the University of the Philippines, Diliman, in 2008. He is currently doing his Ph.D. at the Intelligent Polymer Research Institute, ARC Centre of Excellence for Electromaterials Science, University of Wollongong, Australia. His research interests include the synthesis of graphene, formation of carbon nanocomposites, and the application of these materials for thermal energy conversion systems.

Joselito M. Razal received his Ph.D. degree in Chemistry from The University of Texas at Dallas, USA in 2005. He is now a Senior Research Fellow at the Intelligent Poly- mer Research Institute at the University of Wollongong, Australia. His research interests include synthesis, fabrication and characterization of carbon nanostructures, organic con- ducting polymers and biomaterials, and their applications as novel multifunctional elec- trode materials.

Dennis Antiohos completed a double degree in B.Sci. Photonics and B. Nanotechnol- ogy (Hon.) in 2008. From 2009 to 2010 he spent time in industry working as a Process Engineer and in Continuous Improvement. In 2013 he completed his Ph.D. in Energy Storage at the Intelligent Polymer Research Institute, ARC Centre of Excellence for Elec- tromaterials Science, University of Wollongong, Australia. His research interests include composite materials for the use in energy storage and conversion, as well as technology commercialization.

Gordon Wallace completed his undergraduate (1979) and Ph.D. (1983) degrees at Deakin University. And was awarded a D.Sc. from Deakin University in 2000. He was appointed as a Professor at the University of Wollongong in 1990. He was awarded an ARC Pro- fessorial Fellowship in 2002; an ARC Federation Fellowship in 2006 and ARC Laureate Fellowship in 2011. His research interests include organic conductors, nanomaterials and electrochemical probe methods of analysis and the use of these in the development of intelligent polymer systems. A current focus involves the use of these tools and materi- als in developing biocommunications from the molecular to skeletal domains in order to improve human performance via medical Bionics.

Jun Chen received his Ph.D. degree in chemistry from The University of Wollongong, Australia, in 2003. He is now a Senior Research Fellow at the Intelligent Polymer Research Institute, ARC Centre of Excellence for Electromaterials Science, at the University of Wollongong. His research interests include the design and development of nanostructured composites comprised of electrocatalysts, conducting polymers and carbon nanotubes, and their applications as novel electrode architectures for energy conversion, energy storage, and bioelectrochemistry.

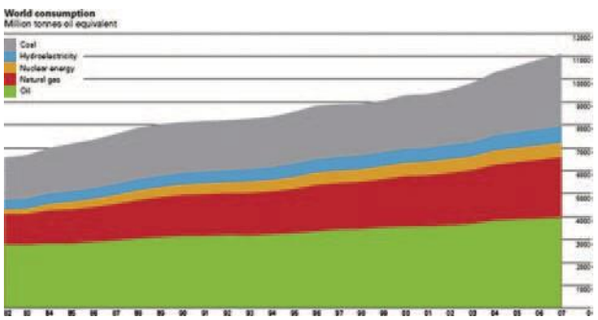

Figure 1. World's energy consumption from 1982 to 2007. Reprinted with permission from [2], G. Giacomelli, *Radiation Measurements* 44, 707 **(2009)**. © 2009, Elsevier Ltd.

is the Wartsila-Sulzer RTA96-C turbocharged two-stroke diesel engine, reputed to be among the most efficient in the world. However, only 50% of the energy in the fuel can be converted to useful motion, with the remainder end- ing up as waste heat.[7] Waste heat is generated in factory operations, particularly from heated product streams, com- bustion gasses that are discharged to the atmosphere and hot equipment surfaces; to name a few. Mining, smelting, paper production, and the extraction of oil and gas are examples of industries that produce excessive waste heat.

1.3. Devices Capable of Harvesting Waste Heat

Progress in the field of low grade thermal energy conversion can lead to more effective use of the ever-present energy source that is waste heat. Devices capable of harnessing waste heat would be able to provide supplemental power to current energy conversion systems and help address the challenges of climate change and the finite nature of fossil fuels.[8] In 1964, Wartanowicz conducted a theoretical analysis on a thermoelectric generator, i.e., a device to convert heat to electrical energy.[9] Since then, other systems capable of transducing waste heat into electrical power have been developed. Examples are ferromagnetic materials, thermocouples and thermionic converters. However, these thermo converters yielded extremely low conversion efficiencies.[10–12] Advances in the more popular thermoelectric devices have been hampered by its high initial cost and material limitations.[13] Another drawback to thermoelectrics is their inflexible nature, limiting their applications to flat surfaces.[14] Scenarios wherein waste heat is generated from curved or irregularly shaped surfaces, i.e., heating/cooling pipes or exhaust pipes on automobiles, would be inapplicable to thermoelectric devices.

Thermogalvanic cells, also known as thermocells are electrochemical systems that can directly transduce thermal energy to electrical power at potentially low cost. These devices have zero carbon emission therefore will not exacerbate environmental issues associated with the generation of electrical power. Long term operation is possible in thermocells without the need for regular maintenance as these devices have no moving mechanical parts; resulting in decreased operational costs. Recently, flexible thermocell electrodes have been developed thus allowing this device to be conformed into various shapes wherein waste heat may be sourced.[15] However, initial studies on thermogalvanic cells result in low power conversion efficiency. Commercial viability of thermocells may be possible if an efficiency relative to a Carnot engine between 2 to 5% is attained.[16] Recent developments in the use of nanocarbons as thermocell electrodes have resulted in significant increases in performance, allowing these devices to attain the target efficiency for commercialization.[17]

2. THERMAL ENERGY HARVESTING

2.1. How a Thermocell Works

A thermocell is a non-isothermal electrochemical cell that is able to directly convert thermal energy to electri- cal power.[18] It has two electrodes that are immersed in a redox based electrolyte. Exposure of the two half-cells of a thermogalvanic system to a thermal gradient induces a difference in redox potentials of the electrolyte at the anode and cathode.[19] This potential difference drives elec- trons through an external circuit and facilitates the produc- tion of electrical energy.[16, 20] Various redox couples have been utilized in thermocell applications, however the best results have been obtained through the use of ferri/ferro cyanide.[21, 22] This is because of the large voltage that is produced at a given temperature difference, also known as the Seebeck coefficient. A schematic of a thermocell with this redox couple is shown in Figure 2.

As can be seen in Figure 2, the oxidation of ferro cyanide allows the extraction of electrons at the anode. These electrons travel through an external circuit and are consumed at the cathode through the reduction of ferri cyanide.[23] Diffusion and convection facilitate the mass transport needed to prevent accumulation of reaction products at either half-cell allowing thermocells to operate in a self-sustaining manner.[16, 24]

As with any heat engine, a thermogalvanic cell is driven by the transport of entropy from a region of elevated temperature to a region of low temperature.[20] The thermoelectric power or Seebeck coefficient ($\Delta V / \Delta T$) of a material is the amount of thermoelectric voltage gener- ated in response to a temperature difference across it. It is

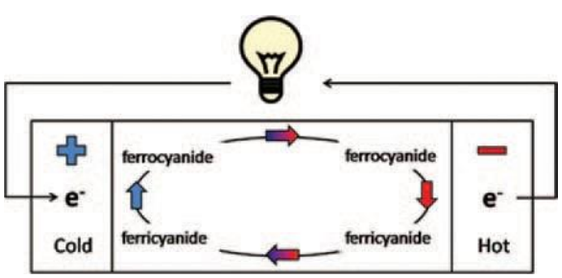

Figure 2. Ferri/ferro cyanide redox thermogalvanic cell.

dictated by the structural entropy induced by ion and solvent interactions.[25] It must be noted that the term thermoelectric power is a misnomer since it is not concerned with power production but instead gives the electric field induced by differences in temperature. Assuming the hypothetical redox system $A + ne^- \rightarrow B$ occurs in the thermo- cell, the Seebeck coefficient may be expressed as shown in Eq. (1).[26]

$$nF\left(\frac{\partial V}{\partial T}\right)_{t=\infty} = \left(S_B + S_B^*\right) - \left(S_A + S_A^*\right) - n\bar{S}_e \qquad (1)$$

Where V represents the electrode potential, T is temperature, S_A and S_B are the partial molar entropies of species A and B accordingly, with their respective Eastman entropies of transport denoted by S_A^* and S_B^*, n is the number of electrons involved in the redox reaction, F is Faraday's constant, and $\bar{S}_e$ is the transported entropy of electrons in the electrodes. The Eastman entropy of transport may be attributed to the interaction of an ion and its hydra- tion shell with the solution. Ions in thermogalvanic cells carry both their partial molar entropy and Eastman entropy of transport into the half-cell as each ion is consumed in one half-cell and produced in the other. It must be noted that Eq. (1) is valid for conditions wherein suffi- cient time has been allowed for the thermocell to reach steady-state. The Seebeck coefficient is initially higher than the steady-state value as molecules around the hot electrode move faster than those surrounding the cold elec- trode, a phenomenon known as the Soret effect. Due to the Soret effect, concentration gradients develop in the ther- mocell wherein the concentration of reactants is higher at the cold side. Despite this, it is common practice to use the initial temperature dependence for two reasons: First, the final steady-state value of the Seebeck coefficient has been shown to take extended periods, even days to be achieved.[27] Second, systems that have a Seebeck coefficient large enough to be useful in thermocells have Eastman entropy of transport values that are small compared to their partial molar entropies.[28] This allows Eq. (1) to be expressed as:[16]

$$nF\left(\frac{\partial V}{\partial T}\right)_{t=0} = S_B - S_A - n\bar{S}_e \qquad (2)$$

For most thermocells, $\bar{S}_e$ is usually infinitesimal. For example, copper leads result in $\bar{S}_e < 2\mu V/°C$.[28] Equa- tion (2) can now be approximated by:

$$\left(\frac{\partial V}{\partial T}\right)_{t=0} \approx \frac{S_B - S_A}{nF} \qquad (3)$$

The power conversion efficiency (η) of a thermocell is given by Eq. (4).[29]

$$\eta = \frac{\text{Electrical power output}}{\text{Thermal power flowing through the cell}} \qquad (4)$$

The thermal power flowing through the cell (Q/T) is largely controlled by cell design and electrolyte selection. It may be expressed as:[30]

$$\frac{Q}{T} = f_i + f_r \qquad (5)$$

Where f_i is the rate of heat flow from the hot electrode to the cold electrode induced by thermal conduction and f_r is the rate of heat transfer induced by the reversible heat of the cell reaction. The expression for the thermal power flowing through the cell can be expanded to give:[28]

$$\frac{Q}{T} = KA\frac{\partial T}{d} + \frac{IT\partial S}{nF} \qquad (6)$$

Where K is the thermal conductivity of the electrolyte, A is the electrode cross sectional area, ∂T is the thermal gradient across the distance (d) between the two electrodes, I is the cell current, ∂S is the entropy of the cell reac- tion, n is the number of electrons transferred and, F is the Faraday constant.

Inclusion of the reversible heat of cell reaction is only valid for thermocells wherein there is a net consumption of electrolyte. For thermogalvanic cells wherein the hot and cold electrodes are periodically switched or when a reversible redox couple is used, no net consumption of the electrolyte occurs. The expression for the thermal power flowing through the cell can be simplified to:[28]

$$\frac{Q}{T} = KA\frac{\partial T}{d} \qquad (7)$$

It has been shown by Anderson et al.[30] that Eq. (7) is a reasonable approximation to Eq. (6) as very little chemical reactions occur in thermocells.

Figure 3 depicts the qualitative behaviour of current and voltage in thermocells with external resistance (r_{ext}).

Based on Figure 3, the maximum electrical output power (P_{max}) is given by Eq. (8).[29]

$$P_{max} = 0.25 V_{OC} I_{SC} \qquad (8)$$

Where V_{oc} is the open circuit voltage and I_{sc} is the short circuit current. Rearranging Eq. (3), we can see that V_{oc} is dictated by the reaction entropy of the redox couple ($\partial S_{B,A}$) and the temperature difference (∂T) to which the half-cells are exposed to as shown in Eq. (9).[16]

$$V_{OC} = \frac{\partial S_{B,A}\partial T}{nF} \qquad (9)$$

The power output of thermogalvanic cells is dictated not only by $\partial V / \partial T$ but also by several overpotentials common in electrochemical cells which will be discussed later on.

Short circuit current densities for thermocells cannot be reliably calculated using the Tafel equation.[31] This is due to the difficulty of reproducibly measuring exchange currents, wherein there is significant variability from one

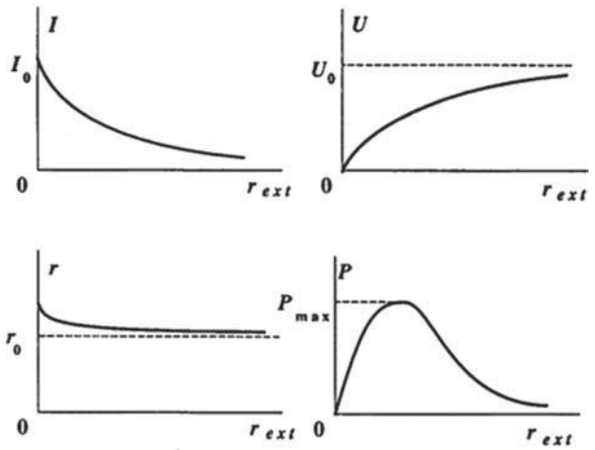

Figure 3. The typical dependencies of the current (I) on the effective voltage (U), internal resistance (r) and the useful power on the exter- nal resistance (r_{ext}) Reprinted with permission from [29], V. S. Artjom, *Electrochim. Acta* 39, 597 **(1994)**. © 1994, Elsevier Ltd.

research group to another. The current generation capability of thermocells is best done by direct measurements. It must be noted that based on the Tafel equation, short circuit current density scales with exchange current densities for thermocells provided that ohmic and mass transport resistance are kept at a minimum.

Using Eqs. (7) and (8), the power conversion efficiency (Eq. (4)) can be expressed as shown in Eq. (10).

$$<P = \frac{0\ 25 V_{OC} I_{SC}}{KA\ \diamond T / d)} \qquad (10)$$

A direct comparison of power conversion efficiency of different power conversion devices would be inaccurate, owing to complications that arise from the difference in operating temperatures used. A convenient method of standardizing power conversion measurements in thermal converters is to compare their power conversion efficiency relative to that of a Carnot engine operating between the same temperatures $<P_r$ (Eq. (11)).

$$<P$$

$$<P_r = \frac{\text{Thermogalvanic cell operating at } \diamond T}{<P_{\text{Carnot engine operating at } \diamond T}} \qquad (11)$$

This facilitates relatively accurate comparisons of thermogalvanic cells having different operating conditions, i.e., thermal gradient, electrolyte, electrode separation, etc.[16]

2.2. Key Factors in Thermocell Efficiency

When current is drawn from an electrochemical cell, the effects on potential difference may be plotted as shown in Figure 4. Said curves describe the current delivery capabilities of fuel cells,[31] storage batteries, photoelectrochemical cells,[32] and thermogalvanic cells.[22, 28] Typical thermocell behaviour would be that represented by the curve ABCD. The effect of activation overpotential accounts for the initial decline in potential difference from the equilibrium

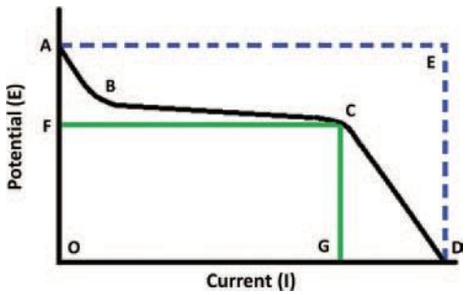

Figure 4. Potential–current (E–I) curves for thermogalvanic cells, ABCD typical, AED ideal cell behaviour.

potential (point A) to point B. The linear portion (point B to point C) is representative of the ohmic overpotential. At high currents, mass transport overpotential effects (drawing current produces net electrode reactions that induce an accumulation of reaction products and depletion of reactants) cause the sharp decrease from point C to point D. For ideal thermocells, (dashed line in Fig. 4) activation overpotential or ohmic overpotential would be negligible so as not to decrease the potential difference delivered by the cell from its equilibrium value. Furthermore, the mass transport overpotential effects are represented by a vertical drop from point E to point D; i.e., mass transport overpotential limits the amount of current that can be drawn from the thermocell.

Consider the behavior of a typical thermocell, the power delivered is maximum at point C. Thermocell power conversion efficiency is at its highest when the area of the rectangle FCGO (subtended by the E–I curve of a typ- ical thermocell in Fig. 4) is maximized.[16] This happens when the potential and amount of current delivered at P_{max} is large. The requirements to ensure maximum thermocell power conversion efficiency are:

(1) an electrolyte that has a high Seebeck coefficient. This will yield a large potential difference for a given temperature gradient; i.e., line OF is larger for electrolytes with a high Seebeck coefficient for a given activation overpotential.[25, 28]

(2) The three overpotentials (activation, ohmic and mass transport) need to be kept to a minimum in order to ensure that the current delivery capability of the thermocell is maximized; i.e., line FC will be as long as possible.[16]

(3) The ratio of the flux of charge carriers between the anode and cathode (electrical conductivity, u) to the flux of heat flowing from the hot to cold electrode (thermal conductivity, K) should be as large as possible. Solvents with low thermal conductivity are ideal.[29]

As mentioned, to ensure maximum current delivery capability, activation, ohmic and mass transport overpotentials need to be kept to a minimum. Ohmic and mass trans- port overpotential may be minimized through electrolyte selection and careful cell design. Our previous work on the effects of ferri/ferro cyanide electrolyte concentration

on thermocell performance revealed that electrolyte conductivity scales with the redox couple concentration.[33] Lower electrolyte resistance is desirable as ohmic overpotential is dominated by electrolyte resistance at large electrode separations. By keeping the electrodes far apart, mass transport overpotential will increase owing to the fact that ions would need to travel a greater distance. However, electrodes should not be positioned too close (despite a decrease in mass transport overpotential) as it will be harder to retain a high thermal gradient in the cell, thus lowering power conversion efficiency.[34] The acti- vation overpotential is dictated by the activation barrier needed for electron transfer and may be mitigated by using catalytic electrodes.[35]

3. RECENT DEVELOPMENTS IN THERMOCELL ELECTRODE MATERIALS

As with most electrochemical systems, initial studies on thermocells utilized platinum electrodes owing to its catalytic properties and non-reactive nature. Power conversion efficiency relative to a Carnot engine of 1.2% was attained using platinum electrodes and a mechanical stirrer to circulate the electrolyte. This external power input is undesirable as it adds considerable cost to the thermoenergy conversion process. Thermogalvanic cells wherein circulation of the electrolyte was not used are only able to attain an efficiency relative to a Carnot engine of around 0.5%.[16] The cost of platinum, together with low power conversion efficiency has kept thermocells from becoming commercially viable.

Large current densities are desirable in thermocells as these result in enhanced power generation capabilities. This may be realized by using a higher concentration of redox mediator in the electrolyte, exposing the electrodes to a larger thermal gradient, and increasing the number of possible sites wherein the redox reactions can occur.[14] This last point may be attained through the use of nano-carbon electrodes.

The discovery of carbon nanotubes (CNTs) in 1991 led to extensive research on this material, particularly in electrochemical applications.[36–43] A CNT could be an individual layer of carbon atoms bonded in a hexagonal lattice that has been rolled up to have a cylindrical shape, this is known as a single-walled carbon nanotube (SWNT). If several layers of carbon atoms are rolled up concentri- cally the resulting structure is called a multi-walled carbon nanotube (MWNT).[44, 45] The nanometer diameter of CNTs, coupled with its unique aspect ratio allows porous electrodes to be fabricated.[46] The specific surface area (SSA) of CNTs falls in the range of 50–1315 m^2/g, depending on the number of walls present.[47–50]

Graphene has a structure similar to CNTs, in the sense that it is composed of a single layer of carbon atoms bonded in a hexagonal lattice.[51–53] However, graphene is not rolled up into a cylinder but instead is an unrolled sheet of carbon.[54, 55] Recent studies have shown that this nano-carbon has exceptional electrical, thermal, mechanical, and optical properties.[53, 56–61] Several "green" technologies are being developed using graphene owing to its unique structure.[62–69] Of note is the SSA of this material which is 2630 m^2/g, making it attractive for energy storage and thermo energy conversion applications.[33, 63, 70]

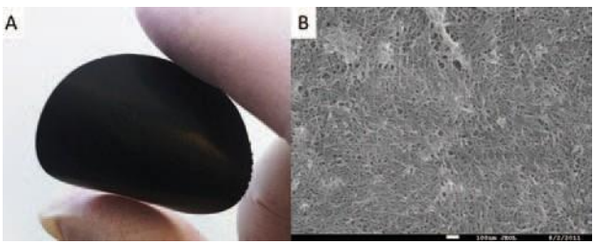

Figure 5. (A) Image, (B) micrograph of a SWNT bucky paper formed by vacuum filtration.

Both CNTs and graphene possess fast electron trans- fer rates with the ferri/ferro cyanide redox couple.[71, 72] As mentioned previously, this redox couple has a relatively high Seebeck coefficient which is why it has been stud- ied extensively in thermocell applications. The high SSA of CNT and graphene allows the fabrication of porous electrodes which possess a large area wherein the redox reactions necessary for thermo energy conversion may occur.[73] These carbon electrodes are also stable over a wide range of temperatures. The combination of these fac- tors allow the generation of large amounts of power in thermocells.

Nano-carbons are normally exfoliated in the liquid phase as their properties are inferior when they are allowed to form aggregates. These nano-carbon dispersions are usually filtered to obtain sheets or bucky papers (Fig. 5) which are used as electrodes in thermocell and other electrochemical applications.[74–77]

3.1. CNTs: SWNT and MWNT Electrodes

The first reported thermocell that utilized carbon electrodes was that developed by Hu et al.[15] A schematic diagram of this device is shown in Figure 6; wherein an electrolyte concentration of 0.4 M ferri/ferro cyanide was employed, electrodes were kept 5 cm apart, T_{hot} 65 °C, and T_{cold} = 4 °C. Using MWNT (less than 1% catalyst and tube diameter 10 nm) bucky paper electrodes with an area of 0.5 cm^2 an areal power density of 1.36 W/m^2 was attained. Platinum electrodes tested using identical conditions produced 33% less power.

Kang et al. developed a vertical thermocell (Fig. 7) wherein the hot electrode (46.4 °C) was oriented above the cold electrode (26.4 °C).[14] The electrodes were kept 4 cm apart with a glass frit separator and 0.2 M ferri/ferro cyanide was used as the electrolyte. They tested SWNT (ASA-100F Hanwha Nanotech, tube diameter 1.3 nm, 20–30 wt.% CNTs, 40 wt.% carbon nanoparticles, 20 wt.%

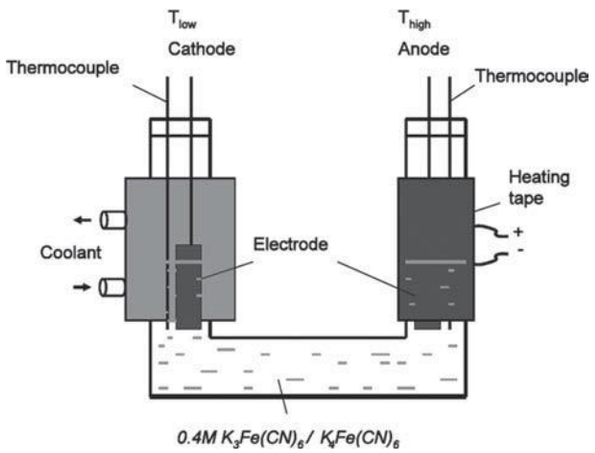

Figure 6. Schematic of the U-Cell used by Hu et al. for thermal harvesting. Reprinted with permission from [15], R. Hu, et al., *Nano Lett.* 10, 838 **(2010)**. © 2010, American Chemical Society.

catalyst material, 10 wt% amorphous carbon and graphite) bucky paper electrodes with an area of 0.25 cm^2 and were able to attain a mass power density of 5.15 W/kg. Ohmic resistance of the SWNT electrode, obtained via electrochemical impedance spectroscopy (EIS) was measured to be 22 *O*.

Using the same conditions and commercially available purified SWNT (P-SWNT, ASP-100F Hanwha Nanotech, 60–70 wt.% nanotubes, 10 wt.% catalyst material, 20 wt.% graphite impurities) a mass power density of 6.8 W/kg was generated. The thermal and acid treatment involved during purification resulted in an ohmic resistance of 21 *O*. This lower resistance of the P-SWNT accounts for the 32% increase in power density as compared to SWNT.

Said group also tested purified MWNT (P-MWNT, SMW100 Southwest Nanotechnologies Inc., 3–6 walls, median tube diameter ~6.6 nm, 98 wt.% carbon) bucky papers. A mass power density (6.13 W/kg) slightly lower than the P-SWNT was attained despite the lower ohmic resistance of 18 *O*. The authors attribute the higher power generated by the P-SWNT to its higher SSA.

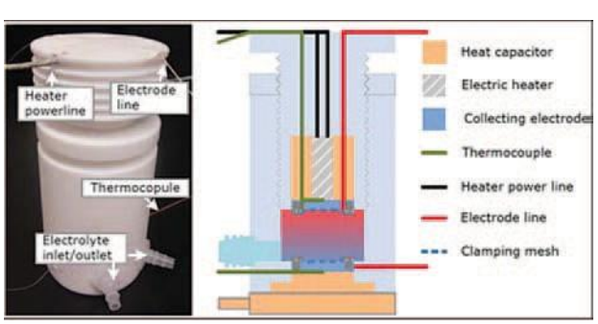

Figure 7. Thermocell used by Kang et al. Reprinted with permission from [14], T. J. Kang, et al., *Adv. Funct. Mater.* 22, 477 **(2012)**. © 2012, John Wiley & Sons, Inc.

3.2. Functionalized CNT Electrodes

The current breakthroughs in CNT research have allowed the functionalization of these carbon materials with specific atoms so as to attain desired properties.[78–80] This process is known as doping.[81] Doping CNTs with nitrogen or boron atoms will enhance certain properties thus facil- itate better performance.[82–84] By doping CNTs with boron (BCNT) an increase in edge plane sites is induced, this increases the rate of electron transfer and increases the catalytic activity.[85, 86] Doping CNTs with nitrogen (NCNT) has been shown to enhance electrocatalytic activity in oxy- gen reactions.[87] Integrating nitrogen atoms into the carbon lattice resulted in additional electrons carriers for the conduction band thus increasing electronic conductivity.[88]

NCNT and BCNT were tested using a U-cell (Fig. 8) with $T_{hot} = 60\ ^{\times}C$ and $T_{cold} = 20\ ^{\times}C$. Electrodes of 0.178 cm^2 were immersed in 0.1 M ferri/ferro cyanide solution.[35] Various symmetric and asymmetric ($NCNT_{hot}$ $BCNT_{cold}$, $BCNT_{hot}$ $NCNT_{cold}$) electrode configurations were tested.

By functionalizing CNTs, an increase in thermocell performance owing to decreased activation overpotential was expected.[14] However, all tests resulted in lower power density for symmetric and asymmetric configurations of the doped electrodes (Fig. 9(A)).[35] It was surmised that the positively charged potassium counter ion of the ferri/ferro cyanide solution ($K_3Fe(CN)_6/K_4Fe(CN)_6$) was repulsed by the positively charged boron atoms.[89] This electro- static repulsion at the electrolyte-electrode interface is reflected in the cyclic voltammogram (CV) of BCNT in the ferri/ferro cyanide solution (Fig. 9(B)). The larger peak separation in the CV of BCNT as compared to CNT is indicative of sluggish electron transfer kinetics.[90] The negative charge of the nitrogen atoms resulted in a high density of the potassium counter ion around the electrodes. This prevented the redox reactions necessary for thermo energy conversion from occurring. This is also reflected in

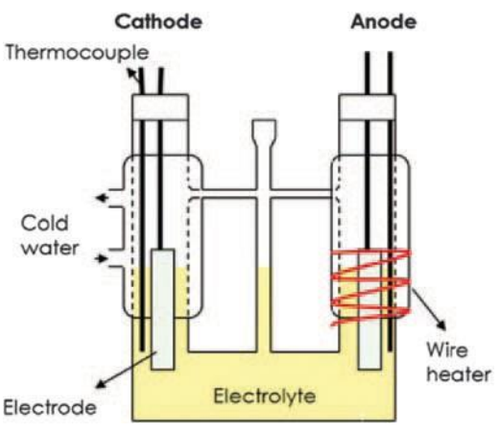

Figure 8. Schematic of the thermocell used by Salazar et al. Repro- duced with permission from [35], P. F. Salazar, et al., *J. Electrochem. Soc.* 159, B483 **(2012)**. © 2012, Electrochemical Society.

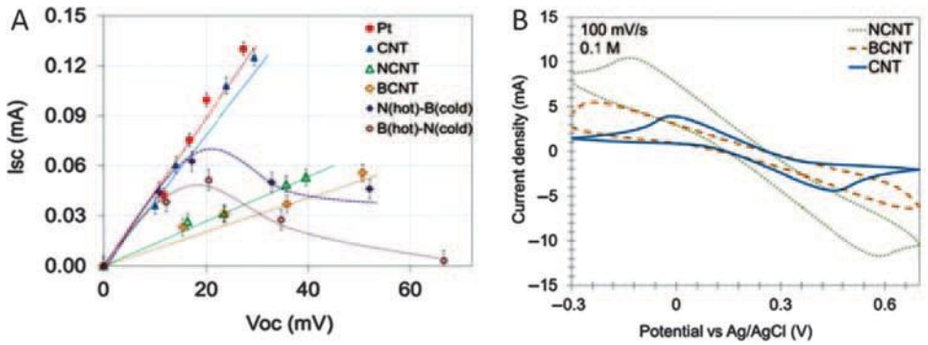

Figure 9. (A) Short circuit current (I_{sc}) against open circuit voltage (V_{oc}) for various electrodes tested by Salazar et al. (B) Cyclic voltammograms of various electrodes tested by Salazar et al. in 0.1 M $K_3Fe(CN)_6$ /$K_4Fe(CN)_6$ run at 100 mV/s versus Ag/AgCl reference electrode. Reproduced with permission from [35], P. F. Salazar, et al., *J. Electrochem. Soc.* 159, B483 **(2012)**. © 2012, Electrochemical Society.

the CV of the NCNT (Fig. 9(B)), which has larger peak separation as compared to CNT.

The asymmetric configurations of NCNT and BCNT depict that at low thermal gradients (less than 14 °C) the short circuit current generated is greater than the symmetric configurations (Fig. 9(A)).[35] Reaction rates at the cold side of the thermocell would be slightly slower than at the hot side, due to faster kinetics at high tempera- tures. With the NCNT at the hot side of the thermocell, the electrolyte surface concentrations are lower owing to the faster kinetics. The slower reaction rates at the cold BCNT electrode results in an accumulation of reactants at this side of the thermocell; thus countering the repul- sive electrostatic effects. These two factors facilitate the production of higher power density. However, at thermal gradients greater than 14 °C the concentration of the potassium counter ion in the vicinity of the NCNT electrode is increased. This results in the "blocking" effect on the NCNT which is detrimental to power generation and is reflected in the decrease of short circuit current. With the NCNT electrode on the cold side, the slower kinet- ics brought about by the lower temperature facilitates the build-up of the potassium counter ion. Hence, the decrease in power generation capabilities is observed at a lower thermal gradient.

3.3. Reduced Graphene Oxide and Composite Electrodes

The use of pristine graphene is impractical for most electrochemical applications as a great amount would be required. One way to obtain large quantities of this is via chemical conversion wherein the graphite is oxidized, exfoliated, and then subsequently reduced.[91, 92] The oxidation step is necessary to make the graphene oxide sheets hydrophilic thus allowing exfoliation.[53] The result- ing material has properties similar to graphene and is known as reduced graphene oxide (rGO). A cross-section of an rGO bucky paper is shown in Figure 10, clearly depicting the sheet like structure of this material.

Kang et al. investigated the use of rGO as electrode materials for thermocells.[14] They employed the same thermocell (Fig. 7) and similar conditions (mentioned in Section 3.1) for the evaluation of SWNT, P-SWNT and P-MWNT as electrodes. Despite the many attractive properties of rGO, it was only able to generate a mass power density of 3.87 W/kg, roughly 57% less than the value attained through the use of P-SWNT. This could be explained by the high ohmic resistance of rGO measured by EIS, which was 35.6 *O*. The ~55% increase in ohmic resistance may be attributed to the residual oxygen containing functional groups on the rGO lattice. Furthermore, the sheet-like structure of rGO may impede diffusion of the redox couple in and out of the electrode. We attained similar results to Kang et al. in our investigation of the effect of electrolyte concentration on thermocell performance using rGO bucky paper electrodes.[33] Using the optimum concentration of 0.4 M ferri/ferro cyanide, a U-shaped cell (Fig. 11), $T_{hot} = 80$ °C and $T_{cold} = 20$ °C, and electrodes sized 1.5 cm × 5 cm we attained a mass power density of 25.51 W/kg. Normalizing the power density to the temperature gradient ($P_{max}/\Delta T^2$) we obtain 7.09×10^{-3} W/kg-K^2, similar to that obtained by Kang et al. (9.68×10^{-3} W/kg-K^2).[14, 33]

The similarities in structure of CNTs and rGO have led to synthesis of composites of these two carbon materials.[93, 94] A wide range of applications has been found for CNT-rGO composites, of note is their performance

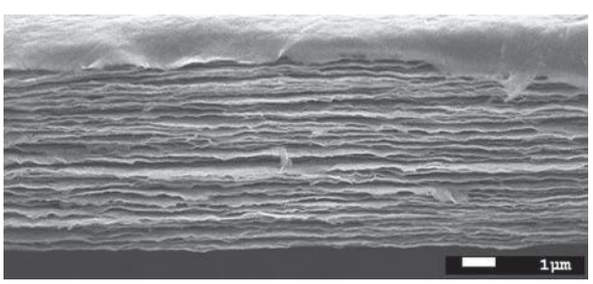

Figure 10. Cross-section of an rGO bucky paper.

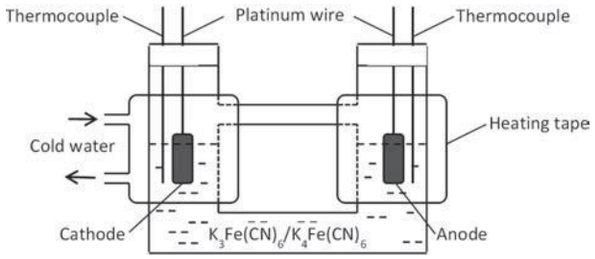

Figure 11. Schematic diagram of the thermocell used by Romano et al. Reproduced with permission from [33], M. Romano, et al., *J. Therm. Anal. Calorim.* 109, 1229 **(2012)**. © 2012, Springer Science Business Media.

as electrodes in electrochemical systems.[95–97] SEM image (Fig. 12) of an SWNT-rGO composite clearly shows the interaction of these two nano-carbons.

PSWNT-rGO composite (1:1 weight ratio) electrodes tested by Kang et al. using the same thermocell and conditions described in Section 3.1 were able to produce amass power density of 5.3 W/kg.[14] Despite a significant improvement in power density compared to the rGO electrode, the composite generates 22% less power than P-SWNT. As mentioned previously, the synthesis of rGO involves oxidizing graphite. The oxygen containing functional groups are not fully removed during the reduction step resulting in defects on the surface of the rGO sheets. These defects resulted in a higher ohmic resistance of the PSWNT-rGO electrode as compared to the P-SWNT which led to inferior thermocell performance. It must be noted that the work performed by Kang et al. was focused on understanding the fundamentals of thermocells employ- ing nano-carbon electrodes. Optimization of the electrode material was not carried out.

In our recent work on SWNT-rGO composites, we optimized the composition and thickness of the thermocell electrode material. SWNTs were sourced from HiPco, Continental Carbon Nanotechnologies Inc. and rGO was synthesized using a modified Hummers method followed

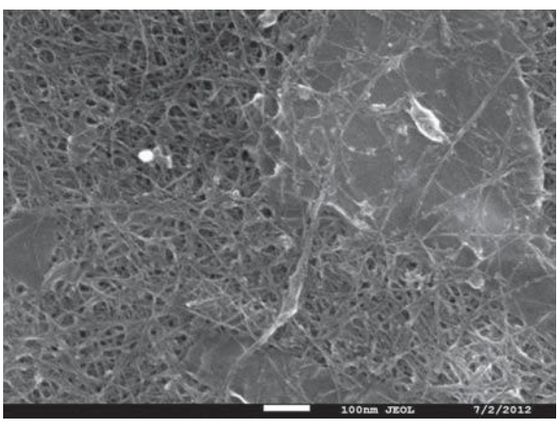

Figure 12. SWNT-rGO composite clearly showing interaction of the two nano-carbons.

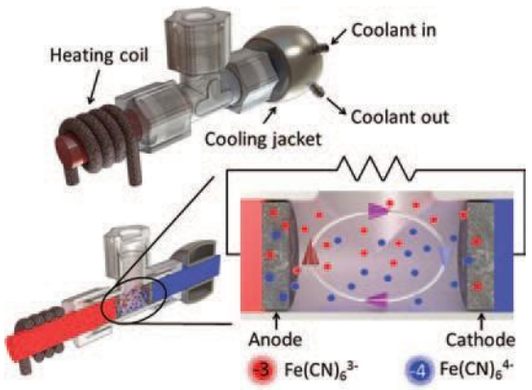

Figure 13. Schematic of the T-cell used by Romano et al. In their investigation of SWNT-rGO composite electrodes. Reproduced with permission from [17], M. S. Romano, et al., *Adv. Mater.* **(2013)**. © 2013, WILEY-VCH Verlag GmbH & Co. KGaA, Weinheim.

by microwave exfoliation. Experiments were carried out using a T-Cell (Fig. 13) with a thermal gradient of ~31 ×C and 0.4 M ferri/ferro cyanide solution.[17] Electrodes are held against stainless steel bars that are heated and cooled by a heating coil and cooling jacket respectively.

Optimization of the nano-carbon composite electrodes revealed that a composition of 90% SWNT and 10% rGO (by weight, henceforth referred to as 90–10) and a thickness of 4.5 μ,m generates the largest areal power density (0.46 W/m^2). This performance may be attributed to the balance between electroactive surface area and film tortuosity of said electrode; i.e., the micro and mesoporos- ity is tailored to maximize the electroactive surface area. CVs (Fig. 14) of the various electrode compositions tested reveal increased faradaic peak current density for the 90– 10 electrode. Since the electrodes display reversible kinet- ics, the increase in faradaic peak currents may be ascribed to increased electroactive surface area.[98]

A comparison of the CVs of the 90–10 electrode of various thicknesses (Fig. 15(A)) shows that the electroac-

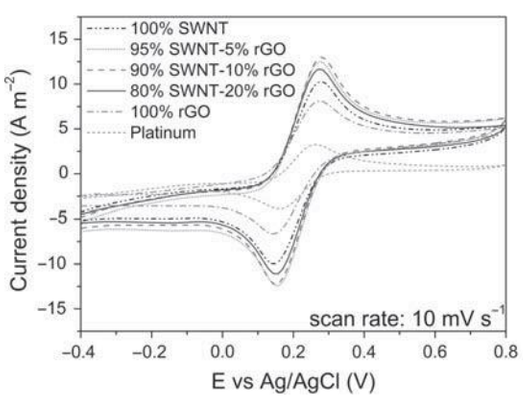

Figure 14. Cyclic voltammograms of the various electrode composi- tions tested by Romano et al. Reproduced with permission from [17], M. S. Romano, et al., *Adv. Mater.* **(2013)**. © 2013, WILEY-VCH Verlag GmbH & Co. KGaA, Weinheim.

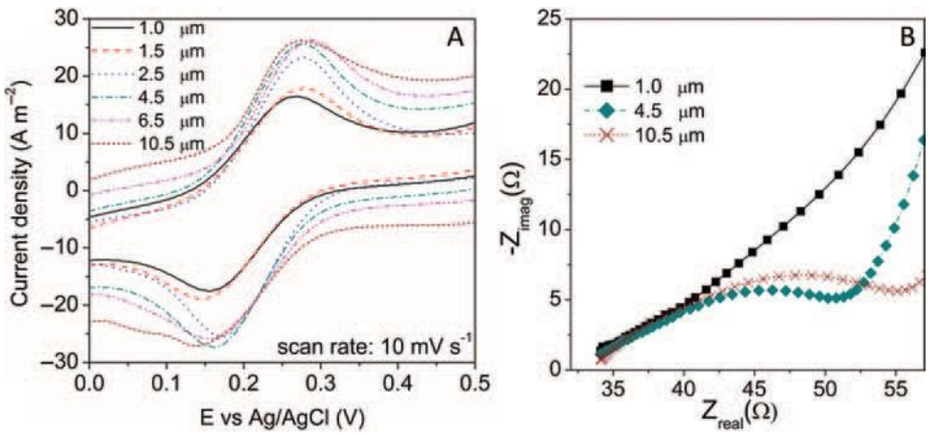

Figure 15. (A) Cyclic voltammograms obtained at 10 mV/s and (B) Nyquist plots generated using 90% SWNT-10% rGO electrodes of increasing thickness. Reproduced with permission from [17], M. S. Romano, et al., *Adv. Mater.* (2013). © 2013, WILEY-VCH Verlag GmbH & Co. KGaA, Weinheim.

tive surface area tapers off at 4.5 μ,m. These results are consistent with the Nyquist plot (Fig. 15(B)) which indicates that charge transfer resistance (R_{ct}, diameter of the semicircle) scales with film thickness. The increased R_{ct} is indicative of the tortuous nature of the 90–10 electrode as film thickness is increased. The random nature of the pores in the electrode results in a meandering path for ions to diffuse, a problem that is exacerbated in thicker films.

4. DEVELOPMENTS IN THERMOCELL AND ELECTRODE DESIGN ATTAINED THROUGH THE USE OF NANO-CARBONS

Research into CNTs and graphene electrode materials has facilitated improvements in thermocell design. The flexible nature of nano-carbons has enabled developments of thermocells that may be wrapped around curved or irregularly shaped surfaces. Nano-carbons may also be grown directly onto thermocell housing so as to decrease contact resistance.[15]

4.1. Flexible Thermocell

Thermocell applications are not limited to situations wherein waste heat is harvested from flat surfaces. Several scenarios exist in which heat may be recovered from irregularly shaped surfaces, such as heating/cooling lines in power plants and car exhaust pipes. One electrode can be placed in contact with the heating/cooling pipe and the other electrode's temperature will be regulated by the ambient. Recently, Hu et al. developed a flexi- ble thermocell.[15] The schematic layout (Fig. 16(a)) shows that two layers of Nomex HT 4848 are used to sepa- rate the two MWNT bucky paper electrodes. The esti- mated distance between electrodes is 2 mm. The entire assembly is encased in a stainless steel sheet and held in place by glue and clamps. 0.4 M ferri/ferro cyanide solution is injected using a syringe to saturate the Nomex separator with electrolyte, after which the hole is sealed. By wrapping the flexible cell around a cooling pipe with a resistive heater then wrapped around it (Fig. 16(b)), an areal power density of 0.039 W/m^2 was generated. A maximum V_{oc} of 21 mV was attained. Using the See- beck coefficient of the electrolyte (1.4 mV/K) the V_{oc} is equivalent to a thermal gradient of 15 $^{\times}$C across the two electrodes. Despite the small separation distance, a rela- tively large temperature gradient was attained because of the Nomex separator used. Through the use of this flex- ible thermocell a $P_{max}/\nabla T^2$ of 1 8 10^{-4} W/m^2-K^2 was achieved. $\times$

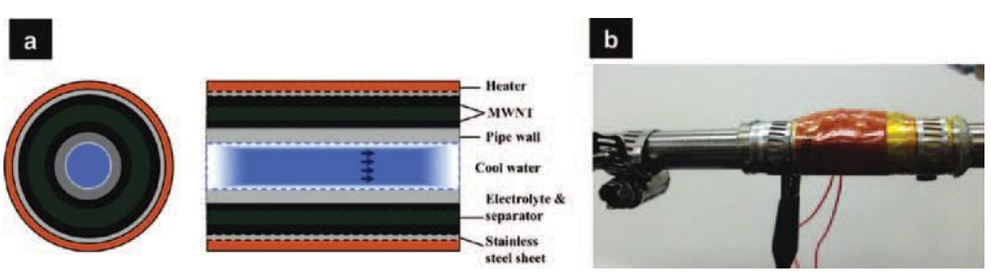

Figure 16. (a) Schematic diagram (b) flexible thermocell covering a cooling pipe with a heater wrapped around it. Reprinted with permission from [15], R. Hu, et al., *Nano Lett.* 10, 838 **(2010)**. © 2010, American Chemical Society.

4.2. Scrolled Electrode Thermocell

As mentioned previously, thermocells using platinum electrodes without circulation of the electrolyte are only able to attain an efficiency relative to a Carnot engine of around 0.5%.[16] This is mainly due to the small surface area available for the redox reactions to occur in platinum. Through the use of MWNT bucky paper scrolled electrodes the relative efficiency was increased by almost three fold; yielding an efficiency of 1.4% relative to a Carnot engine.[15] Aside from the larger electroactive area available in the MWNT bucky paper, it is surmised that the scrolled electrode configuration reduces the heat loss channel. As mentioned in Section 2.2, small interelectrode separations are desir- able as the mass transport overpotential is minimized.[34] However, a shorter distance between electrodes requires a larger thermal input to maintain the same thermal gradi- ent, thus reducing thermocell efficiency. Since the scrolled electrode configuration mitigates heat loss, a large ther- mal gradient can be maintained despite small inter elec- trode separation thus enhancing both mass transport and efficiency. A schematic diagram of the scrolled electrode thermocell is shown in Figure 17. MWNT bucky papers (weighing 0.5 mg) were rolled into a scroll with a diameter of 0.3 cm and placed inside a glass tube. The electrodes were immersed in 0.4 M ferri/ferro cyanide solution and kept 5 cm apart. Using T_{hot} 65 °C and T_{cold} 5 °C, an areal power density of 1.8 W/m^2 was obtained. This corresponds to $P_{max}/\Delta T^2$ of 5 10^{-4} W/m^2-K^2 and a power conversion efficiency of 0.24%.

4.3. Coin Cell

Nano-carbons may be synthesized in various ways, one of which is chemical vapour deposition (CVD). CVD results in the deposition of CNTs or graphene from the gas phase. One advantage of this method in CNT synthesis is that the deposition parameters may be adjusted to obtain highly oriented CNTs on planar substrates.[99]

Thin thermocells; i.e., coin cells (Fig. 18), have been developed with MWNTs grown via CVD.[15] A trilayer catalyst (30 nm Ti, 10 nm Al, 2 nm Fe) was used to grow

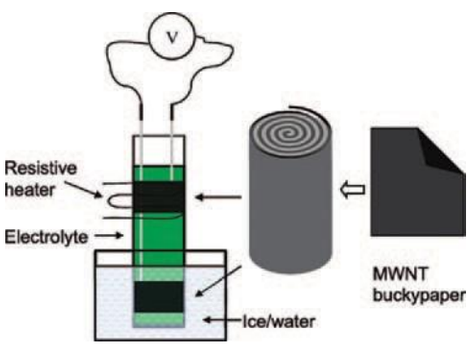

Figure 17. Scrolled electrode thermocell. Reprinted with permission from [15], R. Hu, et. al., *Nano Lett.* 10, 838 **(2010)**. © 2010, American Chemical Society.

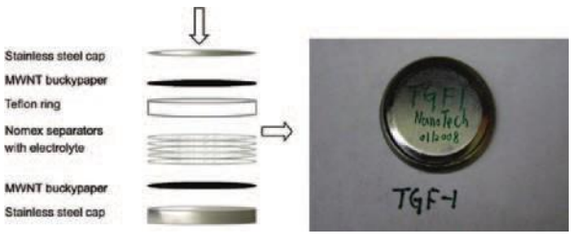

Figure 18. Coin cell for power conversion at low thermal gradients. Reprinted with permission from [15], R. Hu, et al., *Nano Lett.* 10, 838 **(2010)**. © 2010, American Chemical Society.

MWNT forests, around 100 μm tall, directly onto the thermocell casing. Nomex separators impregnated with 0.4 M ferri/ferro cyanide solution was used to keep the elec- trodes apart. Using a 60 °C temperature difference an areal power density of 0.980 W/m^2 was attained. Normalizing the power density to the temperature gradient ($P_{max}/\Delta T^2$) a value of 2 72 10^{-4} W/m^2-K^2 is obtained. Coin cells with MWNT bucky paper electrodes, subjected to a tempera- ture difference of 45 °C produced an areal power density of 0.389 W/m^2. The normalized power density of the coin cell with the bucky paper electrodes (1 92 10^{-4} W/m^2- K^2) is lower than that of the coin cell with MWNTs grown via CVD. The 30% lower power conversion efficiency attained using the MWNT bucky paper electrodes may be attributed to the following: The thermal resistance for MWNT bucky papers is 0.05 cm^2-K/W whereas that of the MWNT forest is only 0.01 cm^2-K/W, this leads to a larger loss of thermal energy at the electrode/thermocell casing junction.[100, 101] Another factor would be the nano- tube alignment in the MWNT forests as this facilitates faster ion diffusion.

4.4. Stacked Electrode Configuration

Using optimized SWNT-rGO composite electrodes (discussed in Section 3.3) a stacked electrode configuration (Fig. 19) was developed to further increase the electroactive surface area of the nano-carbon films.[17] Said configuration consists of alternating layers of stainless steel mesh and the 4.5 μm thick 90–10 electrode. The stainless steel mesh acts as a separator between the SWNT-rGO films, allowing the electrolyte to interact with the high surface area of the nano-carbons while facilitating ionic diffusion. It also maintains a conductive path for electrons between the individual films. The conditions used in thermal har- vesting experiments are stated in Section 3.3. Thermo- cells testing with ten stacked films per half-cell (10-stack configuration) yield a four-fold increase in areal power density (1.85 W/m^2) as compared to a non-stacked config- uration (0.46 W/m^2). The 10-stack configuration attained an efficiency relative to a Carnot engine of 2.63 %. This is currently the largest reported $<P_r$ in thermocells and more importantly is already within the range for commercial viability ($<P_r$ between 2 to 5%).[16]

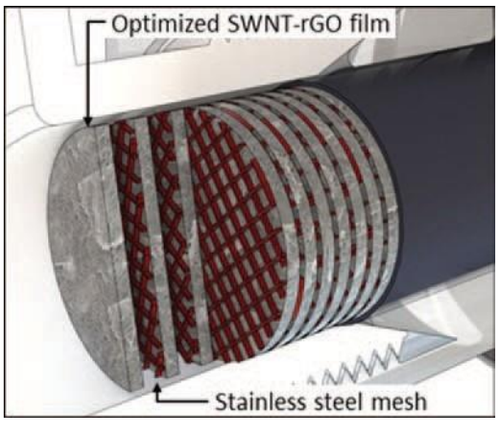

Figure 19. Schematic of the stacked electrode configuration, stainless steel mesh is colored red to differentiate from the SWNT-rGO film. Reproduced with permission from [17], M. S. Romano, et al., *Adv. Mater.* **(2013)**. © 2013, WILEY-VCH Verlag GmbH & Co. KGaA, Weinheim.

5. PERSPECTIVES AND FUTURE DEVELOPMENT

Economic growth of rapidly developing countries will lead to an increase in energy consumption. This will result in the increase in the price of oil, as has been shown in the past few years wherein the cost per barrel ($28 in 2003) went up by more than $50 in three years.[102, 103] Another concern with fossil fuel usage is the pollution that is asso- ciated with fuel extraction, processing and transport.[104] One way to generate "clean" energy is to effectively utilize wasted heat. Current energy conversion systems generate excess heat which may be harvested and used to improve their efficiency.

By using nano-carbon electrode materials the performance of thermocells is significantly enhanced owing to their fast electron transfer kinetics and high surface area. A record power conversion efficiency relative to a Carnot engine of 2.63% was attained through the use of stacked SWNT-rGO composite electrodes.[17] The stacked electrode is structured such that ions may diffuse freely while a high electroactive surface area and good electrical conductivity are maintained. This important breakthrough is made possible by the porous nature of nano-carbon films developed. Furthermore, the excellent mechanical properties and stability in a variety of environments of nano-carbons has led to significant improvements in thermocell design. Flexi- ble thermocells that may be used on irregularly shaped surfaces are now possible. Further developments in ther- mocells, with units arrayed in series may lead to enhanced enhanced voltage output. Developments in nano-carbon synthesis will result in decreased costs of these materi- als. This decreased production cost coupled with improve- ments in thermocell design and electrode properties will allow these devices to harvest low grade heat economi- cally. Commercialization of thermocells will maximize the efficiency of energy systems thus help meet future energy demands.

References and Notes

1. S. A. Kalogirou, *Prog. Energy Combust. Sci.* 30, 231 **(2004)**.
2. G. Giacomelli, *Radiation Measurements* 44, 707 **(2009)**.
3. A. K. Shukla, S. Sampath, and K. Vijayamohanan, *Curr. Sci.* 79, 6 **(2000)**.
4. L. Bengtsson, *Energy Environ.* 17, 755 **(2006)**.
5. M. Kim, S. K. Lee, Y. S. Yang, J. Jeong, N. K. Min, and K. H. Kwon, *J. Nanosci. Nanotechnol.* 13, 7932 **(2013)**.
6. R. Battino and S. E. Wood, Thermodynamics: An Introduction, Academic Press, New York **(1968)**.
7. Wartsila. *The world's most powerful reciprocating engine*. [cited 2012 May]; Available from: http://www. wartsila.com/en/ engines/low-speed-engines/RT-flex96C.
8. T. Murakami, T. Nishikiori, T. Nohira, and Y. Ito, *J. Electrochem. Soc.* 150, A928 **(2003)**.
9. T. Wartanowicz, *Adv. Energy Convers.* 4, 149 **(1964)**.
10. I. Dincer, *Energy and Buildings* 34, 377 **(2002)**.
11. L. E. Bell, *Science* 321, 1457 **(2008)**.
12. M. Ujihara, G. P. Carman, and D. G. Lee, *Appl. Phys. Lett.* 91, 093508 **(2007)**.
13. C. B. Vining, *Nat. Mater.* 8, 83 **(2009)**.
14. T. J. Kang, S. Fang, M. E. Kozlov, C. S. Haines, N. Li, Y. H. Kim, Y. Chen, and R. H. Baughman, *Adv. Funct. Mater.* 22, 477 **(2012)**.
15. R. Hu, B. A. Cola, N. Haram, J. N. Barisci, S. Lee, S. Stoughton, G. Wallace, C. Too, M. Thomas, A. Gestos, M. E.d. Cruz, J. P. Ferraris, A. A. Zakhidov, and R. H. Baughman, *Nano Lett.* 10, 838 **(2010)**.
16. T. I. Quickenden and Y. Mua, *J. Electrochem. Soc.* 142, 3985 **(1995)**.
17. M. S. Romano, N. Li, D. Antiohos, J. M. Razal, A. Nattestad, S. Beirne, S. Fang, Y. Chen, R. Jalili, G. G. Wallace, R. Baughman, and J. Chen, *Adv. Mater.* 25, 6602 **(2013)**.
18. Y. V. Kuzminskii, V. A. Zasukha, and G. Y. Kuzminskaya, *J. Power Sources* 52, 231 **(1994)**.
19. H. G. Hertz and S. K. Ratkje, *J. Electrochem. Soc.* 136, 1698 **(1989)**.
20. A. J. deBethune, T. S. Licht, and N. Swendeman, *J. Electrochem. Soc.* 106, 616 **(1959)**.
21. J. M. Hornut and A. Storck, *J. Appl. Electrochem.* 21, 1103 **(1991)**.
22. K. Shindo, M. Arakawa, and T. Hirai, *J. Power Sources* 70, 228 **(1998)**.
23. R. Goncalves and T. Ikeshoji, *J. Braz. Chem. Soc* 3, 4 **(1992)**.
24. T. I. Quickenden and Y. Mua, *J. Electrochem. Soc.* 142, 3652 **(1995)**.
25. M. Bonetti, S. Nakamae, M. Roger, and P. Guenoun, *J. Chem. Phys.* 134, 114513 **(2011)**.
26. J. N. Agar and W. G. Breck, Trans. *Faraday Soc.* 53, 167 **(1957)**.
27. B. Burrows, *J. Electrochem. Soc.* 123, 154 **(1976)**.
28. T. I. Quickenden and C. F. Vernon, *Sol. Energy* 36, 63 **(1986)**.
29. V. S. Artjom, *Electrochim. Acta* 39, 597 **(1994)**.
30. L. B. Anderson, A. S. Greenberg, and B. G. Adams, Thermally and photochemically regenerative electrochemical systems, Regenerative EMF Cells, American Chemical Society **(1967)**, Vol. 64, p. 213.
31. J. O. M. Bockris and A. K. N. Reddy, Modern Electrochem- istry: An Introduction to an Interdisciplinary Area, Plenum Press **(1970)**.
32. T. I. Quickenden and G. K. Yim, *Sol. Energy* 19, 283 **(1977)**.
33. M. S. Romano, S. Gambhir, J. M. Razal, A. Gestos, G. Wallace, and J. Chen, *J. Therm. Anal. Calorim.* 109, 1229 **(2012)**.
34. Y. Mua and T. I. Quickenden, *J. Electrochem. Soc.* 143, 2558 **(1996)**.
35. P. F. Salazar, S. Kumar, and B. A. Cola, *J. Electrochem. Soc.* 159, B483 **(2012)**.

36. S. Iijima, *Nature* 354, 56 **(1991)**.

37. D. Antiohos, S. E. Moulton, A. I. Minett, G. G. Wallace, and J. Chen, *Electrochem. Commun.* 12, 1471 **(2010)**.

38. B. J. Landi, M. J. Ganter, C. D. Cress, R. A. DiLeo, and R. P. Raffaelle, *Energy Environ. Sci.* 2, 638 **(2009)**.

39. C. Wang, M. Waje, X. Wang, J. M. Tang, R. C. Haddon, and Yan, *Nano Lett.* 4, 345 **(2003)**.

40. R. H. Baughman, A. A. Zakhidov, and W. A. de Heer, *Science* 297, 787 **(2002)**.

41. W. Zhang, P. Sherrell, A. I. Minett, J. M. Razal, and J. Chen, *Energy Environ. Sci.* 3, 1286 **(2010)**.

42. C. Pagura, S. Barison, C. Mortalò, N. Comisso, and M. Schiavon, *Nanosci. Nanotechnol. Lett.* 4, 160 **(2012)**.

43. S. P. Patole, D. W. Shin, B. Fugetsu, and J.-B. Yoo, *J. Nanosci. Nanotechnol.* 13, 7413 **(2013)**.

44. D. Jung, K. H. Lee, D. Kim, L. J. Overzet, and G. S. Lee, *J. Nanosci. Nanotechnol.* 13, 8275 **(2013)**.

45. R. Kotsilkova, E. Ivanov, and V. Michailova, *Nanosci. Nanotechnol. Lett.* 4, 1056 **(2012)**.

46. S. Wang, X. Jiang, H. Zheng, H. Wu, S. J. Kim, and C. Feng, *Nanosci. Nanotechnol. Lett.* 4, 378 **(2012)**.

47. A. Peigney, C. Laurent, E. Flahaut, R. R. Bacsa, and A. Rousset, *Carbon* 39, 507 **(2001)**.

48. S. Inoue, N. Ichikuni, T. Suzuki, T. Uematsu, and K. Kaneko, *J. Phys. Chem. B* 102, 4689 **(1998)**.

49. M. Eswaramoorthy, R. Sen, and C. N. R. Rao, *Chem. Phys. Lett.* 304, 207 **(1999)**.

50. M. H. Koo and H. H. Yoon, *J. Nanosci. Nanotechnol.* 13, 7434 **(2013)**.

51. D. J. Han, K. S. Choi, F. Liu, and T. S. Seo, *J. Nanosci. Nanotechnol.* 13, 8154 **(2013)**.

52. Y. J. Lee, H. W. Park, U. G. Hong, and I. K. Song, *J. Nanosci. Nanotechnol.* 13, 7944 **(2013)**.

53. D. Li, M. B. Muller, S. Gilje, R. B. Kaner, and G. G. Wallace, *Nat. Nano* 3, 101 **(2008)**.

54. K. S. Novoselov, A. K. Geim, S. V. Morozov, D. Jiang, Y. Zhang, S. V. Dubonos, I. V. Grigorieva, and A. A. Firsov, *Science* 306, 666 **(2004)**.

55. D. Su, M. Ren, X. A. Li, and W. Huang, *J. Nanosci. Nanotechnol.* 13, 6471 **(2013)**.

56. M. Lotya, P. J. King, U. Khan, S. De, and J. N. Coleman, *ACS Nano* 4, 3155 **(2010)**.

57. C. Lee, X. Wei, J. W. Kysar, and J. Hone, *Science* 321, 385 **(2008)**.

58. R. R. Nair, P. Blake, A. N. Grigorenko, K. S. Novoselov, T. J. Booth, T. Stauber, N. M. R. Peres, and A. K. Geim, *Science* 320, 1308 **(2008)**.

59. T. Ishihara, Y. Yokoyama, T. Shimosaka, F. Kozono, and H. Hayashi, *Nanosci. Nanotechnol. Lett.* 4, 182 **(2012)**.

60. X. You, J. Kim, Y. K. Pak, and J. J. Pak, *J. Nanosci. Nanotechnol.* 13, 7349 **(2013)**.

61. Y. J. Yun and K. B. Song, *J. Nanosci. Nanotechnol.* 13, 7376 **(2013)**.

62. K. I. Bolotin, K. J. Sikes, Z. Jiang, M. Klima, G. Fudenberg, J. Hone, P. Kim, and H. L. Stormer, *Solid State Commun.* 146, 351 **(2008)**.

63. M. D. Stoller, S. Park, Y. Zhu, J. An, and R. S. Ruoff, *Nano Lett.* 8, 3498 **(2008)**.

64. Q. Wu, Y. Xu, Z. Yao, A. Liu, and G. Shi, *ACS Nano* 4, 1963 **(2010)**.

65. E. Yoo, J. Kim, E. Hosono, H. S. Zhou, T. Kudo, and I. Honma, *Nano Lett.* 8, 2277 **(2008)**.

66. G. M. Scheuermann, L. Rumi, P. Steurer, W. Bannwarth, and R. Mülhaupt, *J. Am. Chem. Soc.* 131, 8262 **(2009)**.

67. J. T. Robinson, F. K. Perkins, E. S. Snow, Z. Wei, and P. E. Sheehan, *Nano Lett.* 8, 3137 **(2008)**.

68. S. Park, N. Mohanty, J. W. Suk, A. Nagaraja, J. An, R. D. Piner, W. Cai, D. R. Dreyer, V. Berry, and R. S. Ruoff, *Adv. Mater.* 22, 1736 **(2010)**.

69. Y. Xu, Q. Wu, Y. Sun, H. Bai, and G. Shi, *ACS Nano* 4, 7358 **(2010)**.

70. X. Li, H. Song, K. Du, Y. Zhang, and J. Huang, *Nanosci. Nanotechnol. Lett.* 4, 191 **(2012)**.

71. J. M. Nugent, K. S. V. Santhanam, A. Rubio, and P. M. Ajayan, *Nano Lett.* 1, 87 **(2001)**.

72. L. Tang, Y. Wang, Y. Li, H. Feng, J. Lu, and J. Li, *Adv. Funct. Mater.* 19, 2782 **(2009)**.

73. K. Jiang, L. Ma, J. Wang, and W. Chen, *Rev. Nanosci. Nanotechnol.* 2, 171 **(2013)**.

74. J. Liu, A. G. Rinzler, H. Dai, J. H. Hafner, R. K. Bradley, P. J. Boul, A. Lu, T. Iverson, K. Shelimov, C. B. Huffman, F. Rodriguez-Macias, Y. S. Shon, T. R. Lee, D. T. Colbert, and R. E. Smalley, *Science* 280, 1253 **(1998)**.

75. H. Z. Geng, D. S. Lee, K. K. Kim, G. H. Han, H. K. Park, and Y. H. Lee, *Chem. Phys. Lett.* 455, 275 **(2008)**.

76. C. K. Lee, S. B. Lee, S. W. Hwang, K. W. Park, and J. K. Shim, *J. Nanosci. Nanotechnol.* 13, 7391 **(2013)**.

77. H. Lu and J. Gou, *Nanosci. Nanotechnol. Lett.* 4, 1155 **(2012)**.

78. H. H. Park, Y. Choi, B. Kim, Y. S. Yun, and H. J. Jin, *J. Nanosci. Nanotechnol.* 13, 7950 **(2013)**.

79. M. D. A. Sayeed, Y. H. Kim, Y. Park, A. I. Gopalan, K. P. Lee, and S. J. Choi, *J. Nanosci. Nanotechnol.* 13, 7424 **(2013)**.

80. M. K. Seo, Y. S. Kuk, and S. J. Park, *J. Nanosci. Nanotechnol.* 13, 7920 **(2013)**.

81. L. S. Panchakarla, A. Govindaraj, and C. N. R. Rao, *ACS Nano* 1, 494 **(2007)**.

82. K. Y. Chun, H. S. Lee, and C. J. Lee, *Carbon* 47, 169 **(2009)**.

83. J. C. Charlier, M. Terrones, M. Baxendale, V. Meunier, T. Zacharia, N. L. Rupesinghe, W. K. Hsu, N. Grobert, H. Terrones, and G. A. J. Amaratunga, *Nano Lett.* 2, 1191 **(2002)**.

84. C. Deng, J. Chen, X. Chen, M. Wang, Z. Nie, and S. Yao, *Electrochim. Acta* 54, 3298 **(2009)**.

85. C. E. Banks and R. G. Compton, *Analyst* 130, 1232 **(2005)**.

86. C. Deng, J. Chen, X. Chen, C. Xiao, Z. Nie, and S. Yao, *Electrochem. Commun.* 10, 907 **(2008)**.

87. K. Gong, F. Du, Z. Xia, M. Durstock, and L. Dai, *Science* 323, 760 **(2009)**.

88. M. Terrones, P. M. Ajayan, F. Banhart, X. Blase, D. L. Carroll, J. C. Charlier, R. Czerw, B. Foley, N. Grobert, R. Kamalakaran, P. Kohler-Redlich, M. Rühle, T. Seeger, and H. Terrones, *Appl. Phys. A: Materials Science and Processing* 74, 355 **(2002)**.

89. D. Strmcnik, K. Kodama, D. van der Vliet, J. Greeley, V. R. Stamenkovic, and N. M. Marković, *Nat. Chem.* 1, 466 **(2009)**.

90. M. Pacios, M. del Valle, J. Bartroli, and M. J. Esplandiu, *J. Electroanal. Chem.* 619–620, 117 **(2008)**.

91. D. C. Marcano, D. V. Kosynkin, J. M. Berlin, A. Sinitskii, Z. Sun, A. Slesarev, L. B. Alemany, W. Lu, and J. M. Tour, *ACS Nano* 4, 4806 **(2010)**.

92. W. S. Hummers and R. E. Offeman, *J. Am. Chem. Soc.* 80, 1339 **(1958)**.

93. S. H. Jung, W. Song, S. I. Lee, Y. Kim, M. J. Cha, S. H. Kim, D. S. Jung, M. W. Jung, K. S. An, and C. Y. Park, *J. Nanosci. Nanotechnol.* 13, 6730 **(2013)**.

94. D. H. Nam, S. I. Cha, Y. J. Jeong, and S. H. Hong, *J. Nanosci. Nanotechnol.* 13, 7365 **(2013)**.

95. L. Qiu, L., X. Yang, X. Gou, W. Yang, Z. F. Ma, G. G. Wallace, and D. Li, *Chemistry—A European Journal* 16, 10653 **(2010)**.

96. S. Y. Yang, K. H. Chang, H. W. Tien, Y. F. Lee, S. M. Li, Y. S. Wang, J. Y. Wang, C. C. M. Ma, and C. C. Hu, *J. Mater. Chem.* 21, 2374 **(2011)**.
97. Q. Su, Y. Liang, X. Feng, and K. Mullen, *Chem. Commun.* 46, 8279 **(2010)**.
98. A. J. Bard and L. R. Faulkner, Electrochamical Methods-Fundamentals and Applications, 2nd edn., John Wiley and Sons, New York **(2001)**.
99. J. Chen, Y. Liu, A. I. Minett, C. Lynam, J. Wang, and G. G. Wallace, *Chem. Mater.* 19, 3595 **(2007)**.
100. P. Myounggu, A. C. Baratunde, S. Thomas, X. Jun, R. M. Matthew, S. F. Timothy, and K. Hyonny, *Nanotechnology* 17, 2294 **(2006)**.
101. B. A. Cola, J. Xu, C. Cheng, X. Xu, T. S. Fisher, and H. Hu, *J. Appl. Phys.* 101, 054313 **(2007)**.
102. L. Noam, *Energy* 35, 2631 **(2010)**.
103. B. M. Fronk, R. Neal, and S. Garimella, *J. Energy Resour. Technol.* 132, 021009 **(2010)**.
104. J. A. Turner, *Science* 285, 687 **(1999)**.